

Time resolved simultaneous small- and wide-angle X-ray scattering during polyethylene deformation – II. Cold drawing of linear polyethylene

Michael F. Butler^a, Athene M. Donald^{a,*} and Anthony J. Ryan^{b,c}

^aDepartment of Physics, Cavendish Laboratory, University of Cambridge, Madingley Road, Cambridge CB3 0HE, UK

^bMaterials Science Centre, UMIST, Grosvenor Street, Manchester M1 7HS, UK

^cCCLRC Daresbury Laboratory, Daresbury, Warrington WA4 4AD, Cheshire, UK
 (Received 10 December 1996)

The cold drawing behaviour of a range of unoriented linear polyethylenes was investigated using the technique of simultaneous small- and wide-angle X-ray scattering during deformation. The influences of molecular weight and thermal history were studied. The role of both variables was found to be highly important since by altering the percentage crystallinity they influenced the relative amounts of inter- and intra-lamellar deformation. The micromechanical deformation processes governing the different regions of the load-extension curve were found to be the same as for cold-drawn ethylene- α -olefin copolymers, demonstrating the fundamental similarity between all types of unoriented polyethylene PE. © 1997 Elsevier Science Ltd.

(Keywords: X-ray scattering; linear polyethylene; cold drawing)

INTRODUCTION

This paper is the second in a series of three reporting the findings from an investigation into the micromechanical behaviour of a range of commercial grade polyethylenes deformed at room temperature. In the first paper¹ the properties of a range of ethylene- α -olefin copolymers were described. This paper aims to investigate the influence of molecular weight on the interaction between the molecular and lamellar deformation mechanisms and its role in determining the macroscopic deformation. This was achieved by simultaneously measuring the small- and wide-angle X-ray scattering (SAXS and WAXS, respectively) patterns and the load-extension curve *in situ* during deformation for a range of cold-drawn linear polyethylenes. A study of polydisperse commercial grade materials is a valid investigation of the influence of molecular weight since it has been demonstrated that the results from fractionated polymers can be qualitatively extrapolated to polydisperse systems².

It is known that thermal history and molecular weight exert marked influences on the mechanical properties of linear polyethylene^{2–6}. Studies of the macroscopic behaviour have shown that, at constant molecular weight the yield stress increases with percentage crystallinity and that for a given thermal history, the yield stress increases with increasing molecular weight². The higher yield stress in the more crystalline samples results from the increased amount of crystalline material which can support higher stresses

than the amorphous component. In the second case, as molecular weight is increased, a greater number of tie molecules and physical entanglements are formed. These allow the interlamellar regions as well as the lamellae to support higher stresses. Longer chains are also less mobile, and during crystallization they form lamellae with more disordered fold surfaces. A more disordered fold surface hinders the chain slip process and the pulling out of chain folds contributing to lamellar deformation. Therefore, the effect of increasing the molecular weight is to reduce the contribution to the overall deformation of the crystalline lamellae, and vice versa.

The wealth of experiments on the mechanical properties of polyethylene have shown that melt-crystallized materials qualitatively behave in a similar manner to each other, and that both the amorphous and crystalline components are involved in the deformation^{7,8}. Initial elastic deformation is accommodated by a combination of the following processes: lamellar separation, interlamellar shear and lamellar stack rotation. Plastic deformation follows, and has been identified as due to the operation of a variety of mechanisms involving the crystalline lamellae. Commonly identified mechanisms are: chain slip, in which the molecules slide past each other parallel to their length; transverse slip, in which the slip direction is perpendicular to the chain axis; deformation twinning; and a stress induced martensitic transformation, in which the stable orthorhombic phase is sheared to form a metastable monoclinic one. In unoriented PE, many of these mechanisms coexist, making it difficult to elucidate the sequence of deformation mechanisms leading to the final fibrillar texture.

Additional complexity is provided by the relaxation that inevitably occurs after a sample is released from load so that

* To whom correspondence should be addressed. Tel.: (+44) (0)1223 337007; Fax (+44) (0)1223 337000

many experiments do not study the material in its fully deformed state. This makes it especially difficult to study the elastic deformation processes, since the tie molecules permeating the rubbery amorphous component that link adjacent lamellae make elastic deformation almost entirely reversible^{9,10}. The high flux of synchrotron X-ray radiation overcomes this problem by enabling real-time microstructural studies to be performed during deformation. The technique is further strengthened by the simultaneous measurement of the load–extension curve with the X-ray scattering patterns, which enables the molecular, lamellar and macroscopic deformation to be precisely correlated.

EXPERIMENTAL SECTION

Materials and sample preparation

A range of linear polyethylenes with different molecular weights and polydispersities, supplied by BP Chemicals Ltd., were used in this study. *M_w* values lay between 60 000 and 1 500 000. Sample information is summarised in Table 1. Samples A and B may be defined as high-density polyethylene (HDPE), D and E as high molecular weight high-density polyethylene (HMW–HDPE) and sample F as an ultra-high molecular weight high-density polyethylene (UHMW–PE). These classifications will be used later in the discussion of the results.

Plaques, 0.9 mm thick, were formed by compression moulding the molten PE using the method described previously¹¹. Specially shaped samples for tensile testing were punched from these plaques. They were 50 mm long and 20 mm wide, with two semi-circular cut-outs of radius 8 mm to ensure that yielding always occurred in the beam.

Some samples were annealed in vacuum at (132 ± 1)°C for 22 h in order to change the percentage crystallinity, lamellar thickness and lamellar population. They were then cooled slowly (initial cooling rate 0.5°C/min) to room temperature. The annealed samples are denoted by SC, and the unannealed ones by U, to match previous notation.

Differential scanning calorimetry

Differential scanning calorimetry (DSC) was used to obtain the percentage crystallinity of the samples and information on the lamellar populations and thicknesses. Measurements were taken on a Perkin Elmer DSC7 equipped with an Intracooler II and calibrated with indium and zinc. The lamellar thickness, *L_c*, was estimated by rearranging the equation for the melting point, *T_m*

$$L_c = \frac{2\sigma_e}{\Delta h} \frac{T_{m0}}{(T_{m0} - T_m)} \tag{1}$$

Using the value of (93 ± 8) × 10⁻⁷ J/cm² for the fold surface energy, *σ_e*¹² employing 280 J/cm³ for the heat of fusion of crystal, *Δh*¹², and taking the equilibrium melting temperature, *T_{m0}*, to be equal to 145.8°C¹², lamellar thicknesses were estimated.

Table 1 Sample information

Sample	Type	<i>M_w</i> /1000	<i>M_w</i> / <i>M_n</i>
A	HDPE	60	4.7
B	HDPE	131	6.3
D	HMW–HDPE	311	8.6
E	HMW–HDPE	385	9.0
F	UHMW–PE	1500	unknown

The percentage crystallinity was calculated from the specific heat of fusion by taking the specific heat of fusion of perfectly crystalline PE to be 293 J/g¹³. An estimate for the lamellar thickness from the SAXS long spacing, *d*, was made using the two phase model from the lamellar thickness, *L_c*, and the percentage crystallinity, *χ*, for comparison with DSC results

$$L_c = \chi d \tag{2}$$

Simultaneous SAXS/WAXS measurement during in situ deformation

X-ray scattering experiments were performed on beam-lines 2.1¹⁴ and 16.1^{15,16}, at the Synchrotron Radiation Source (SRS) at Daresbury in the United Kingdom, with the set-up described and illustrated previously^{1,11}. Two-dimensional SAXS and WAXS patterns were obtained simultaneously during deformation using gas filled multiwire area detectors from the highly deformed necked region of the sample. Because it was only possible to collect a portion of the WAXS pattern with the multiwire area detector, two separate samples were used to collect the equatorial and meridional portions of the WAXS patterns separately. Analysis of the peak intensities was performed within the region of the WAXS pattern indicated previously¹¹. Samples were drawn at an extension rate of 5.0 mm/min in a Rheometrics Ltd, Miniature Materials Tester.

Image plates were used to collect the full wide-angle diffraction pattern for some samples drawn at 1 mm/min. The sample was exposed to the X-ray beam at selected points on the load–extension curve. Unannealed samples E and F which had just yielded were allowed to relax without load and examined approximately 1 h later.

The Lorentz correction^{17,18} which corresponds to multiplying the intensity by *q*², where *q* is the scattering vector, was applied to all the SAXS data. The scattering vector is taken to be

$$|q| = q = \frac{2\pi}{d} = \frac{4\pi}{\lambda} \sin \theta \tag{3}$$

where *d* is the long spacing, *λ* the X-ray wavelength and *θ* the scattering angle.

RESULTS

DSC

DSC curves, showing the melting transition, are shown in Figure 1 for annealed sample E. All of the untreated and annealed samples had one melting endotherm, indicating a

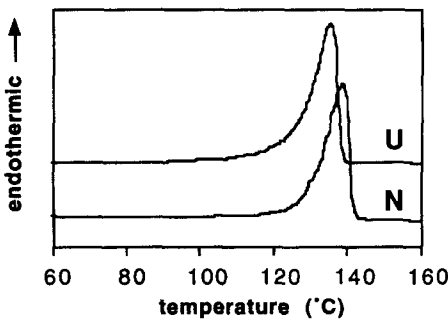


Figure 1 DSC curves from sections of undeformed (U) and necked (N) annealed HMW-HDPE sample E

Table 2 Information from DSC

Sample	Undeformed			Necked	
	T_m (°C)	L_c (nm)	% cryst.	T_m (°C)	% cryst.
A u	134.2 ± 0.4	24.0 ± 2.1	70.2 ± 0.3	n/m	n/m
A sc	138.5 ± 0.8	38.2 ± 3.3	78.0 ± 1.4	–	–
B u	135.1 ± 0.1	26.0 ± 2.2	74.9 ± 0.1	137.4 ± 0.5	58.7 ± 0.5
B sc	139.0 ± 0.4	35.7 ± 3.1	79.6 ± 0.6	137.2 ± 0.5	71.9 ± 0.5
D u	135.0 ± 0.3	25.6 ± 2.2	63.8 ± 0.5	134.6 ± 0.1	58.2 ± 0.6
D sc	138.3 ± 0.4	36.9 ± 3.2	72.1 ± 0.2	136.3 ± 0.3	62.8 ± 0.7
E u	135.2 ± 0.1	26.2 ± 2.3	65.4 ± 0.8	136.3 ± 0.6	57.3 ± 0.7
E sc	138.1 ± 0.1	36.1 ± 3.1	78.7 ± 0.2	138.2 ± 0.5	69.6 ± 0.5
F u	134.3 ± 0.1	24.2 ± 2.1	49.8 ± 0.4	135.0 ± 0.1	45.9 ± 1.4
F sc	133.7 ± 0.1	23.0 ± 2.0	53.0 ± 0.4	134.7 ± 0.5	47.5 ± 0.5

unimodal lamellar thickness population. Table 2 shows the information derived from the DSC experiments for all of the samples.

Percentage crystallinity decreased with increasing molecular weight. Annealing increased the percentage crystallinity and caused lamellar thickening. Drawn specimens were less crystalline than the undeformed ones and generally had higher melting points than the undrawn material (see Figure 1). The drawn samples melted over a smaller temperature range than the undrawn ones (see Figure 1), as did the annealed compared to the unannealed specimens.

Tensile properties

A ductile–brittle transition occurred upon decreasing the molecular weight and increasing the percentage crystallinity. The untreated HDPE and the HMW–HDPE and UHMW–PE samples with both thermal histories were ductile. Samples BU, DU, DSC, EU, ESC and FSC formed stable necks whereas sample FU deformed homogeneously. Annealed A was brittle and fractured, whereas unannealed A and annealed B formed unstable necks, as reported previously for sample B¹¹, which were unable to sustain high strains. Yield points, defined as a maximum in the load–extension curve, were exhibited by all of the samples except for unannealed F, which showed only an elastic response followed by a plateau. In all cases, the annealed samples had sharper yield points than their untreated counterparts.

WAXS

Peak intensities

The WAXS patterns from the undeformed samples showed that in all cases the crystalline regions adopted the stable orthorhombic unit cell (which has been indexed previously)¹¹. The evolution of the equatorial intensities of the orthorhombic reflections was directly related to the load–extension curve, and followed the same behaviour for all molecular weights and thermal histories, which was also the same as the HDPE, MDPE and LLDPE samples reported previously^{1,11}. Figure 2 shows a sequence of equatorial WAXS patterns along with the simultaneously obtained load–extension curve and SAXS patterns. A sequence of meridional WAXS and SAXS patterns recorded at similar strains but from a different sample (with the simultaneously obtained load–extension curve) is shown in Figure 3.

The meridional scattering gradually disappeared as the

reflections oriented towards the equator. Equatorial reflections at higher scattering angles also became much weaker. The similar evolution of the equatorial peak intensities with strain for all of the samples is shown in Figure 4. Changes in the peak intensities occurred more rapidly for the lower molecular weight and more crystalline samples. The evolution of the orthorhombic peak intensities is correlated with the load–extension curve and the results from SAXS, shown in Figure 5 for untreated B, untreated E and untreated F (in order to compare HDPE, HMW–HDPE and UHMW–PE). The other samples gave similar results.

In the first stages of elastic deformation all of the intensities remained constant. Changes in intensity began at the yield point on the load–extension curve (defined as the maximum in load) and proceeded until strain softening (the reduction in load with increasing extension) ceased. During strain softening the orthorhombic (110) and (020) reflections decreased in intensity and the orthorhombic (200) intensity increased slightly. Upon reaching the plateau region of the load–extension curve the intensities remained roughly constant. The orthorhombic (110) intensity increased slightly for the HMW–HDPE and UHMW–PE samples, E and F, respectively, but remained constant for the HDPE samples A and B. The most pronounced difference between thermal histories was for the UHMW–PE sample F, in which the changes were much more rapid in the annealed specimen. There was a greater amount of elastic deformation and the changes in intensity occurred at higher strains in the higher molecular weight samples.

During deformation, extra reflections appeared in all of the samples, except for annealed A, coincident with the yield point on the load–extension curve. They can be seen in the 2D patterns in Figures 2 and 3. These new reflections were identified as arising from the monoclinic phase, indexing as $(\bar{2}01)$, $(200)_z$, (001) and (210) (using $a = 8.09$ Å, $b = 2.53$ Å, $c = 4.79$ Å), indicating that a stress-induced martensitic transformation had occurred and initiated at the yield point. The (001) peak was the strongest of the monoclinic reflections, and is clearly shown in the meridional WAXS inside the main orthorhombic reflections in Figure 3.

The strain at which the monoclinic (001) and $(\bar{2}01)$ reflections first appeared in the equatorial and meridional portions of the WAXS pattern was taken to be the strain at which the martensitic transformation had been activated. It is shown in Table 3, as the value ϵ_m , for all of the samples. The values ϵ_v , ϵ_{110} and ϵ_y are the strain at which cavitation occurred, the strain at which the orthorhombic (110) reflection developed into a four point pattern and the

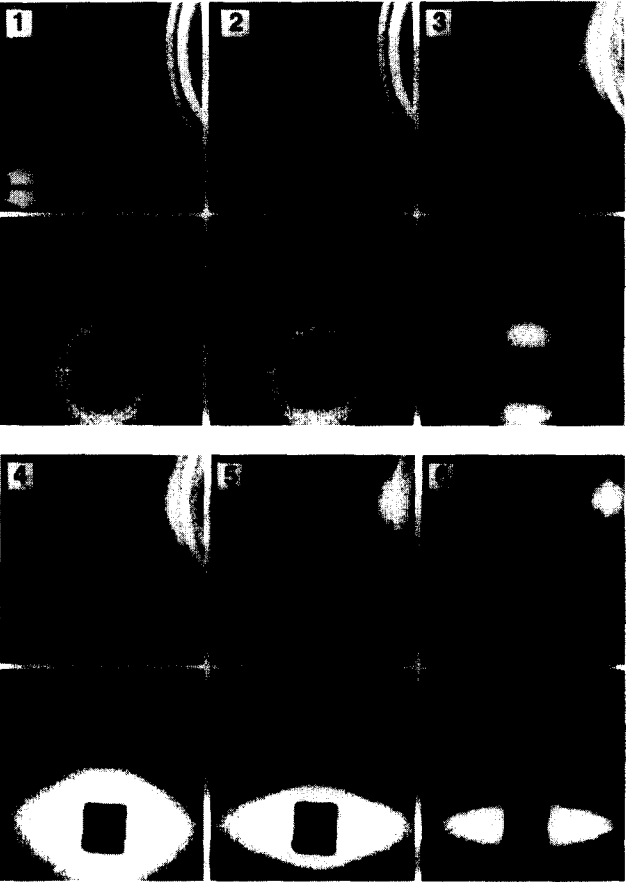
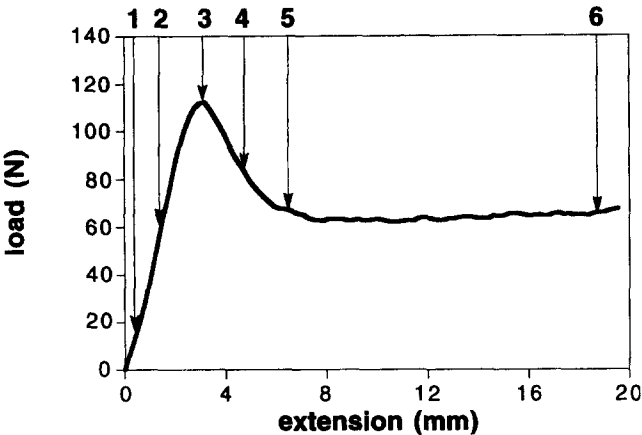


Figure 2 Simultaneously obtained SAXS and equatorial WAXS patterns and load-extension curve for unannealed HDPE sample B. The tensile axis is indicated by the double-headed arrow. The monoclinic reflections that appeared at the yield point are also arrowed

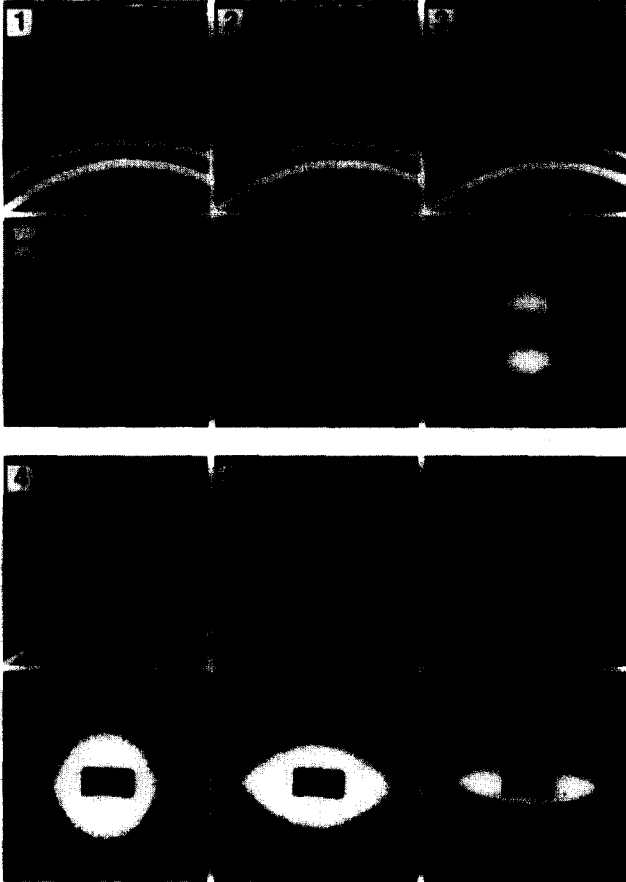
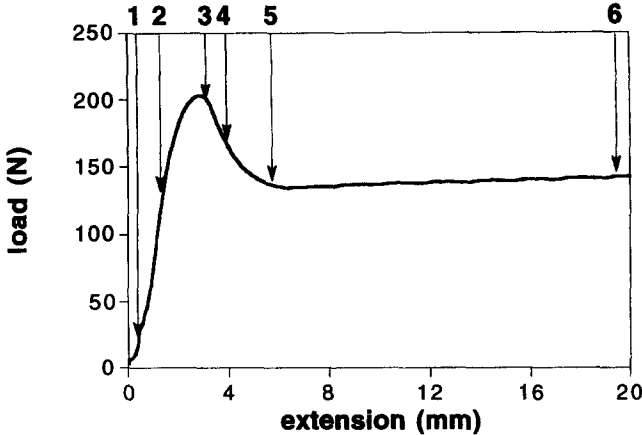


Figure 3 Simultaneously obtained SAXS and meridional WAXS patterns and load-extension curve for unannealed HDPE sample B. The tensile axis is indicated by the double-headed arrow. The monoclinic reflections that appeared at the yield point are also arrowed

Table 3 Correlations between the martensitic transformation strain (ϵ_m), cavitation strain (ϵ_v), orthorhombic (110) four point pattern strain range (ϵ_{110}) and the yield strain (ϵ_y)

Sample	ϵ_m	ϵ_v	ϵ_{110}	ϵ_y
A u	0.095 ± 0.038	0.095 ± 0.038	—	0.098
B u	0.170 ± 0.038	0.170 ± 0.038	0.170–0.208	0.135
B sc	0.095 ± 0.038	0.095 ± 0.038	—	0.090
D u	0.132 ± 0.038	0.132 ± 0.038	0.208–0.360	0.136
D sc	0.095 ± 0.038	0.095 ± 0.038	0.133–	0.115
E u	0.133 ± 0.038	0.133 ± 0.038	0.170–0.284	0.139
E sc	0.095 ± 0.038	0.095 ± 0.038	0.133–0.246	0.079
F u	0.170 ± 0.038	0.170 ± 0.038	0.208–0.167	
F sc	0.095 ± 0.038	0.095 ± 0.038	0.095–	0.065

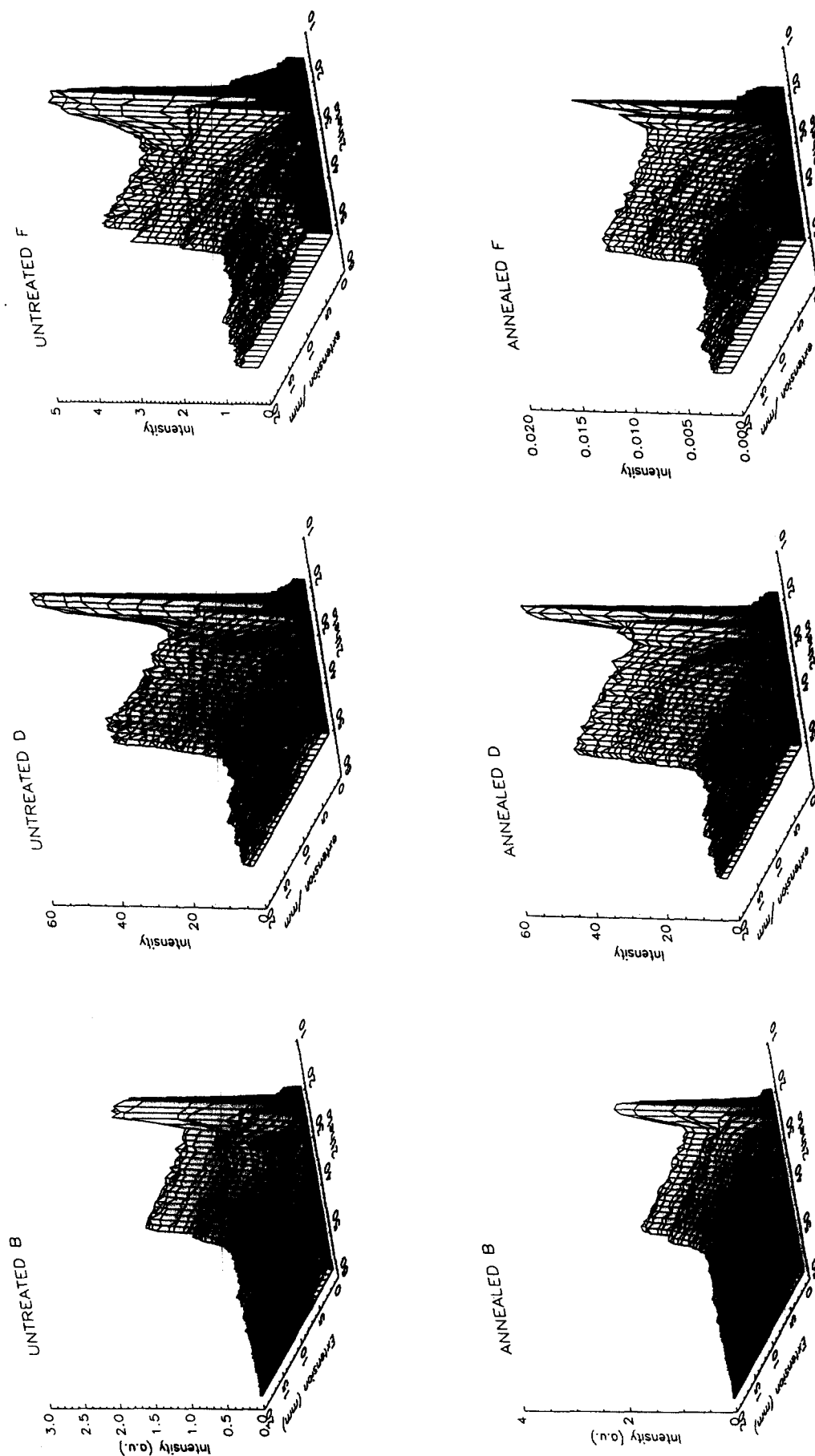


Figure 4 3D intensity plots showing the evolution of the equatorial WAXS intensity profiles with strain for annealed and unannealed HDPE, HMW-HDPE and UHMW-PE. The basic similarity in behaviour, regardless of molecular weight, is clearly apparent

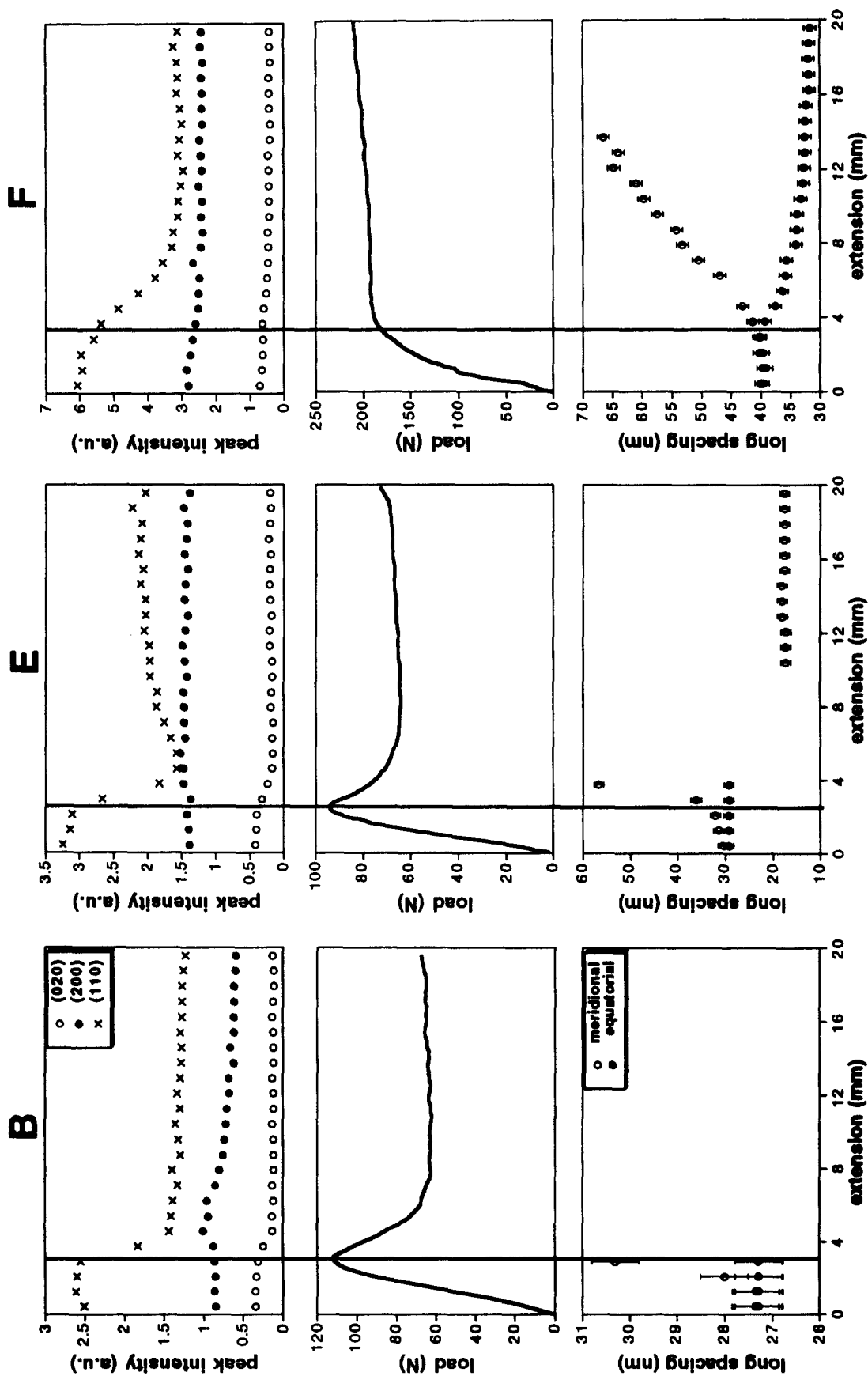


Figure 5 Correlation of the WAXS peak intensities, SAXS long spacings and load-extension curves for HDPE, HMW-HDPE and UHMW-PE. Equatorial long spacings were overwhelmed by the yield point for HDPE and HMW-HDPE

strain at the yield point, respectively. Although cavitation is discussed later, the strain at which voids formed is placed in *Table 3* to demonstrate the correlation between the small- and wide-angle scattering. From *Table 3*, it is obvious that thermal history had an effect on the deformation behaviour. Annealed samples underwent the stress-induced martensitic transformation and yielded at lower strains than the untreated samples. With the exception of slow-cooled F, it can also be seen that the martensitic transformation occurred at higher strains as molecular weight increased.

The monoclinic ($\bar{2}01$) reflection increased in intensity until a certain strain was reached, which corresponded to the start of the plateau in the load extension curve. In most of the samples the monoclinic ($\bar{2}01$) intensity then remained constant, but in untreated D and E it decreased as deformation continued, in the same way as for annealed HDPE B described earlier¹¹. As found previously for HDPE, MDPE and LLDPE, the increase in the monoclinic ($\bar{2}01$) intensity was accompanied by a decrease in the intensity of the orthorhombic (110) and (020) peaks for all HDPE, HMW-HDPE and UHMW-PE samples. This decrease in intensity of the orthorhombic (110) peak was correlated with the increase in intensity of the monoclinic ($\bar{2}01$) peak. The reflections at larger scattering angles virtually disappeared.

Orientation of the reflections

During deformation all of the reflections became less isotropic as the PE chains became increasingly aligned with the tensile axis, shown in *Figures 2 and 3*. No discernible orientation occurred until the yield point was reached, whereupon the orthorhombic (200) reflection began to orient towards the equator, forming an equatorially centred arc. Significant orientation of the orthorhombic (110) and (020) reflections (hence the yield point) began at a lower strain and occurred more rapidly for the lower molecular weight and more crystalline samples. No orientation was observed for the most crystalline, lowest molecular weight, annealed sample A which fractured before yield. In unannealed A and annealed B the orthorhombic (110) reflection proceeded rapidly to an equatorially centred arc with the formation of an unstable neck. Orientation of the orthorhombic (110) reflection towards the equator proceeded via a four point pattern for the less crystalline and higher molecular weight ductile samples (unannealed B and unannealed and annealed D, E and F). The strain range over which the four point pattern was observed is given in *Table 3* as ϵ_{110} . It can be seen that the formation of the four point pattern occurred after the yield point for cold-drawn HDPE, HMW-HDPE and UHMW-PE. It persisted during strain softening before evolving into an equatorially centred arc at some strain in the load-extension plateau, with the exception of sample F which retained the four point pattern. The four point pattern was better defined for the higher molecular weight samples (D, E and F). The influence of molecular weight on the orientation is shown in *Figure 6* in which a comparison is made between samples A, E and F drawn at 1.0 mm/min to an extension of 25 mm. The sample with the lowest M_w achieved a two point fibre pattern whereas the sample with the highest M_w retained the orthorhombic (110) four point pattern. For the intermediate M_w sample the reflections were equatorially centred arcs.

Unlike the orthorhombic reflections, the monoclinic reflections were not initially isotropic, as can be seen in *Figure 7*, which is the complete WAXS pattern recorded at the yield point for unannealed HMW-HDPE sample E. The

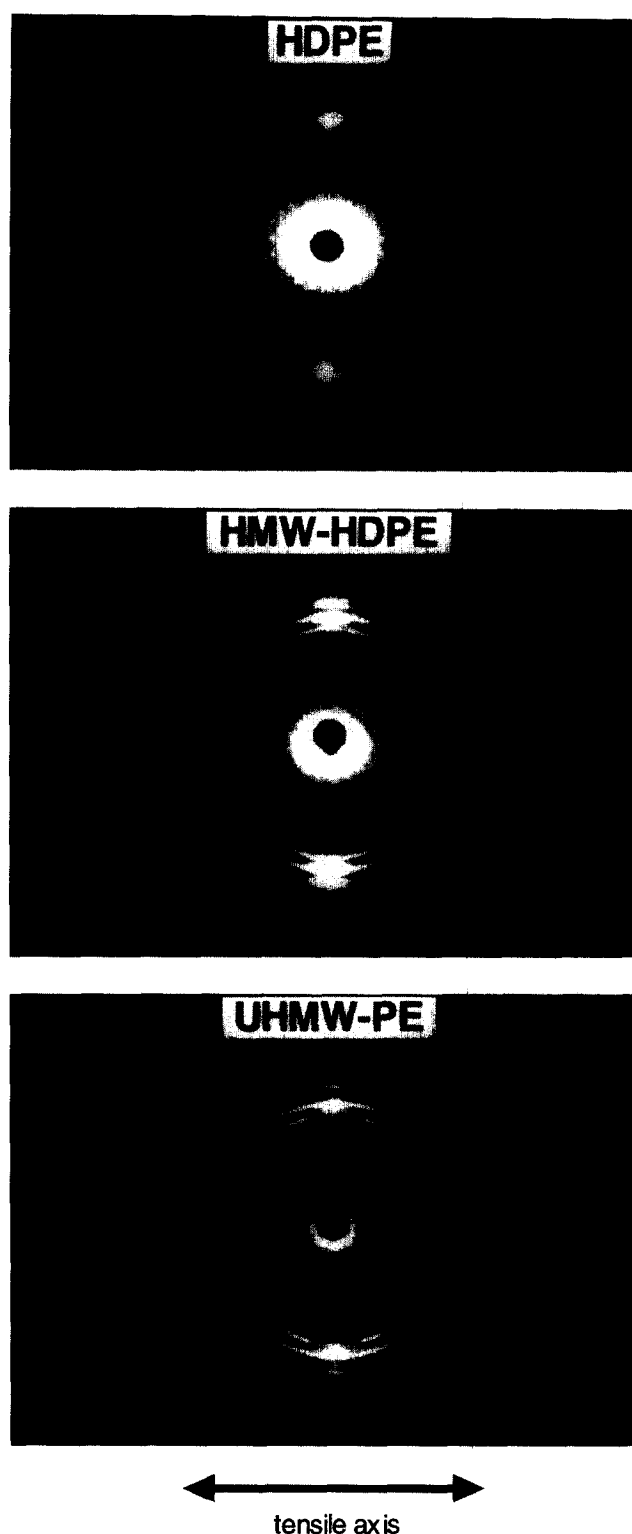


Figure 6 WAXS patterns of necked HDPE, HMW-HDPE and UHMW-PE, drawn to the same extension, indicating the influence of molecular weight on the attainable molecular orientation during tensile deformation

monoclinic (001) reflection was initially a very broad arc centred on the meridian. It progressed to a four point pattern and then to a fibre pattern. It was observed that the orthorhombic (110) reflection became an equatorially centred arc before the monoclinic (001) reflection did. The weaker monoclinic (020) reflection developed as a four point pattern which gradually aligned on the equator, whereas the monoclinic ($\bar{2}01$) reflection appeared and remained on the equator. For this reason the ($\bar{2}01$) intensity was used as an indication of the onset and extent of the

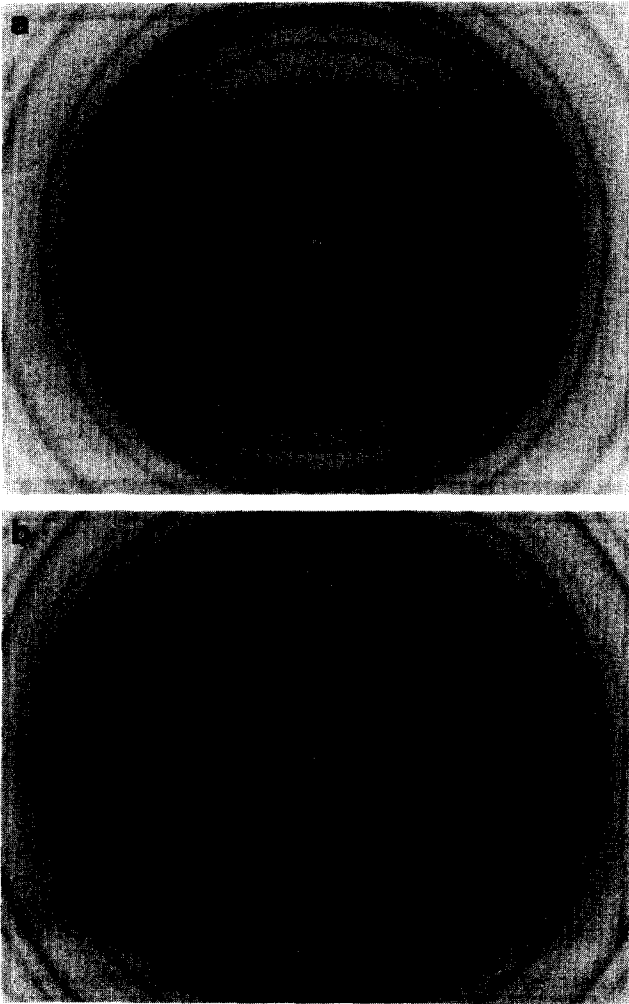


Figure 7 (a) WAXS pattern at the yield point for HMW-HDPE. (b) WAXS pattern taken 1 h after release from load, showing the disappearance of the monoclinic phase upon stress-relaxation

martensitic transformation, as its intensity was less affected by orientation effects than the (001) and (020) reflections. As for the orthorhombic reflections, the monoclinic reflections transformed to the fibre pattern or equatorially centred arcs except in sample F, for which the (020) and (001) remained as four point patterns (see Figure 6). It was found that the HMW-HDPE and UHMW-PE samples

Table 4 Long spacing measured by SAXS (d_{SAXS}) and calculated from DSC (d_{DSC}) and the constant ratio between them

Sample	d_{SAXS}	d_{DSC}	$d_{\text{SAXS}}/d_{\text{DSC}}$
A U	24.7	33.5 ± 4.1	0.737 ± 0.120
A sc	34.9	38.7 ± 3.3	0.902 ± 0.077
B U	27.1	40.1 ± 3.4	0.675 ± 0.057
B sc	41.5	55.8 ± 7.0	0.744 ± 0.126
D U	29.6	40.2 ± 3.5	0.736 ± 0.064
D sc	37.2	51.2 ± 4.4	0.727 ± 0.062
E U	29.4	40.9 ± 5.1	0.719 ± 0.126
E sc	40.5	54.5 ± 6.75	0.743 ± 0.124
F U	39.6	48.6 ± 4.2	0.815 ± 0.070

drawn to the yield point, at which point the WAXS pattern resembled Figure 7a, and then unloaded, returned to a similar orientation to the undeformed samples. A WAXS pattern from a yielded and relaxed sample is shown in Figure 7b. No monoclinic reflections were visible and there was no discernible orientation of the orthorhombic reflections for these samples.

SAXS

At least one peak was present in the SAXS patterns from all of the samples, which was attributed to scattering from lamellae. Annealed samples exhibited second order peaks, indicating their greater degree of crystalline perfection. The SAXS long spacing information from the undeformed samples agreed qualitatively, but not quantitatively, with the DSC results and both are shown in Table 4 for comparison. This point has been discussed before in ref. ¹.

Sequences of SAXS patterns from sample B recorded during deformation are shown in Figures 2 and 3. Figure 8 compares sequences of SAXS patterns obtained from samples E and F, recorded at the same strains, in order to compare HMW-HDPE and UHMW-PE. The long spacings measured from both the equatorial and meridional scattering profiles are given in Figure 5, where they are correlated with the information from WAXS and the load-extension curve. During elastic deformation there was no change in the equatorial long spacing. The meridional long spacing was observed to increase before the yield point for all of the samples except for unannealed F, in which the increase began at the yield point. The meridional long spacing increased by the largest amount for unannealed F. The yield point also coincided with the onset of a decrease

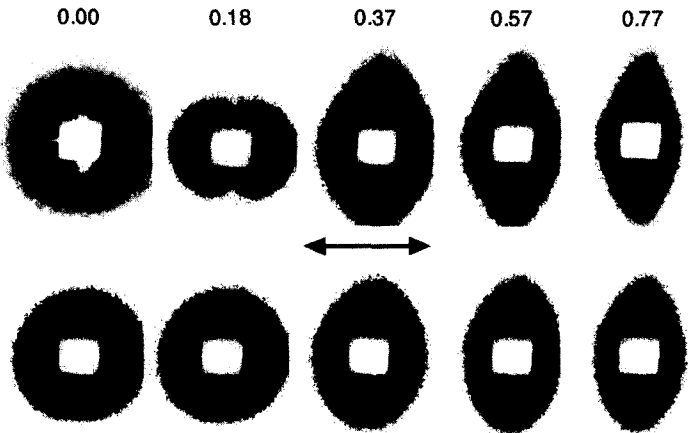


Figure 8 SAXS patterns from unannealed HMW-HDPE sample E (top) and unannealed UHMW-PE sample F (bottom) measured at the strains shown, for comparison with the SAXS patterns shown in Figures 2 and 3 which were from HDPE. The tensile axis is arrowed. The void scattering is much better defined in the lower molecular weight HMW-HDPE, especially on the meridian at the onset of cavitation (0.18 strain)

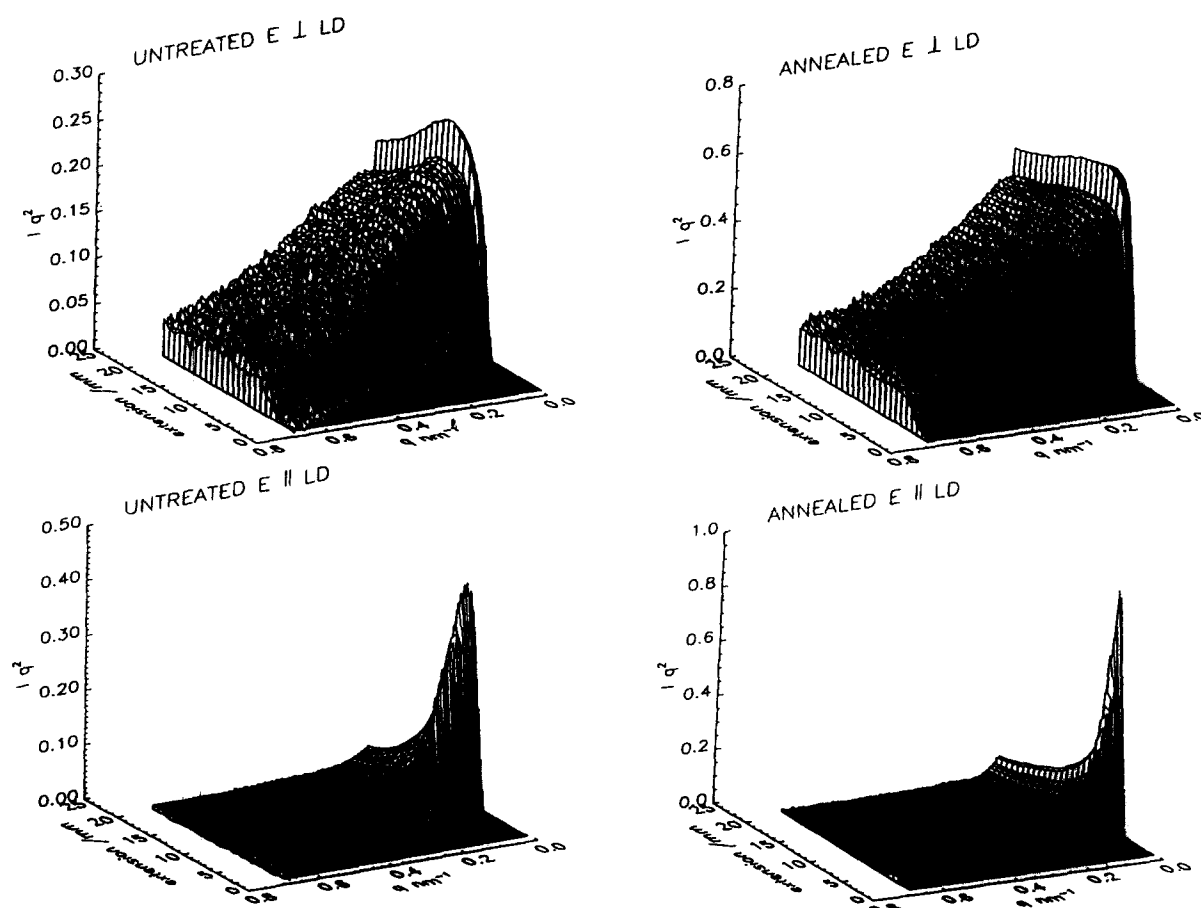


Figure 9 Evolution of the meridional (perpendicular to LD) and equatorial SAXS intensity (parallel to LD) profiles during deformation for annealed and unannealed HMW-HDPE sample E. Note the onset of cavitation at a lower strain and the greater intensity of void scattering in the annealed sample

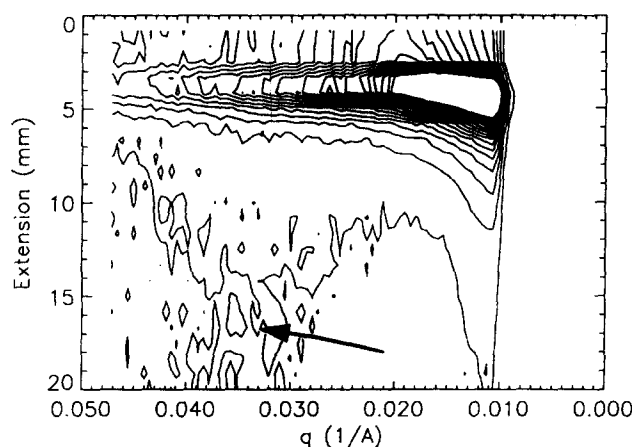


Figure 10 Contour plot of the evolution of meridional SAXS intensity with deformation for HMW-HDPE sample E, with the weak peak from the fibrillar structure arrowed

in the equatorial long spacing in unannealed and annealed sample F. For the other samples, lamellar scattering was overwhelmed by void scattering which began at the yield point. Cavitation occurred in all of the samples which led to a dramatic increase in the SAXS intensity and whitening of the deformed region. The greatest amount of voiding occurred in samples with the lowest molecular weight.

Equatorial and meridional SAXS intensity profiles are shown in Figure 9 for untreated and annealed HMW-HDPE sample E, as a typical example. The sudden onset of

cavitation, obscuring all traces of lamellar scattering, can be clearly seen. The strains at which the voids were formed, ϵ_v , taken as the strain at which the SAXS intensity began to increase markedly, are given in Table 3. It can be seen that the onset of cavitation coincided with the onset of the stress-induced martensitic transformation and the macroscopic yield point. Therefore, cavitation occurred at higher strains in the less crystalline and higher molecular weight samples. At high strains in the untreated HMW-HDPE, during the load-extension plateau, a fibre pattern was discerned from a very weak maximum in the meridional SAXS profile. Figure 10 is a contour plot of the meridional scattering for untreated E, showing the very weak broad maximum. Despite having fewer voids, a fibre pattern was not discerned in untreated F.

From Figures 2, 3, 8 and 9 it can be seen that the void scattering initially manifested itself on the meridian, where it gave rise to an intense spot in the same q range as the lamellar scattering. The void scattering very rapidly disappeared from the meridian and concentrated upon the equator, forming the equatorial streak seen in Figures 2, 3, and 8. Comparison of the UHMW-PE with the HMW-PE in Figure 8 and the HDPE in Figures 2 and 3 shows that the void scattering was less pronounced for the UHMW-PE. This correlated with a reduced amount of whitening observed in the deformed region of the UHMW-PE. The equatorial SAXS intensity resulting from cavitation increased during strain softening, coinciding with the increase in amount of monoclinic material, reaching a constant value which was maintained during the plateau. As

deformation progressed the streak became longer and narrower (see Figures 2, 3, and 8).

DISCUSSION

DSC

Although there is a discrepancy between the values of lamellar thickness given by SAXS and DSC, DSC remains useful to confirm the structural information given by SAXS. It is again argued that the difference in long spacing measured by SAXS and DSC, found also for LLDPE and MDPE samples¹, may be attributed to the value of the fold surface energy of $(93 \pm 8) \times 10^{-7} \text{ Jcm}^{-2}$ used in equation (1) to calculate the lamellar thickness from the melting temperature being inaccurate. The linear PE samples had the same ratio of SAXS to DSC long spacing, averaged to 0.734 ± 0.062 , regardless of thermal history. Fitting this value of fold surface energy to match SAXS and DSC long spacings gives a value $(68 \pm 6) \times 10^{-7} \text{ Jcm}^{-2}$ for the fold surface energy of the HDPE samples studied. Similar values have been reported for isothermally crystallized bulk PE¹⁹, which suggests that they are more relevant to bulk material than the widely used value of $(93 \pm 8) \times 10^{-7} \text{ Jcm}^{-2}$.

The larger long spacings, detected by SAXS, of the annealed samples compared with the unannealed ones are explained by lamellar thickening since DSC shows the annealed samples to possess thicker lamellae. The accompanying increase in percentage crystallinity with annealing is expected because annealing reduces the number of defects in the crystal structure as well as increasing the amount of crystalline material by lamellar thickening¹³.

A decrease in percentage crystallinity upon drawing was previously attributed to stress-induced decrystallization¹. Since strain-induced crystallization cannot occur if the chains relax²⁰, the results, which showed that the decrease in percentage crystallinity only occurred in samples in which voids formed, suggest that stress-induced decrystallization results from local stress relaxation caused by the formation of voids. The presence of strained tie molecules and aligned molecules in all samples is indicated by the increased melting temperatures of the deformed specimens^{21,22}.

Deformation mechanisms

Elastic deformation. The constant WAXS and SAXS peak intensities and lack of discernible orientation of the crystalline reflections during elastic deformation indicate that this region of the load-extension curve is dominated by deformation of the amorphous component. The increase in meridional long spacing in this region is due to interlamellar separation²³⁻²⁹. Lack of deformation of the lamellae themselves is indicated by the constancy of the meridional SAXS intensity profile, which would be expected to change if lamellar disruption occurred. Comparison of the linear polyethylenes used in this study with the ethylene- α -olefin copolymers described previously¹ showed a greater amount of lamellar separation in the more crystalline linear PE. There is probably less disentanglement resistance in the linear polyethylenes owing to the reduced amount of amorphous material, with fewer entanglements per chain and fewer tie molecules, which allows the lamellae to separate more readily. The constant equatorial long spacing suggests that interlamellar shear and/or rotation, both of which by themselves have negligible effects on the interlamellar spacing, occur for lamellar stacks with their normals inclined to the tensile axis.

The yield point. Previous workers have inferred, from the dependence of the yield stress on the percentage crystallinity, that yielding results from crystallographic deformation^{2-6,30-33}. The four major changes in both the SAXS and WAXS that began at the yield point in this study confirmed that the macroscopic yield point resulted from yielding of the crystalline lamellae. These four observations were the onset of crystalline orientation, the decrease in equatorial long spacing, the activation of the martensitic transformation and the onset of cavitation, all of which occurred at the yield point.

The onset of orientation in the WAXS pattern at the yield point provides evidence for the deformation of the crystalline component. Orientation of the WAXS reflections along the equator signifies that the molecules in the lamellae align parallel to the tensile axis³⁴. The orientation of the orthorhombic (200) reflection has been proposed to be due to (110) twinning followed by (100)[001] chain slip³⁵. Interlamellar shear is proposed to play a role in the rapidity of the orientation of this reflection³⁶. Although deformation twinning cannot be identified from the results, (100)[001] slip is the chain slip mode that is theoretically most easily activated, and has been identified in unoriented HDPE using detailed pole figure analyses by other workers³⁶⁻³⁸.

The chain slip mode is identified by the decrease in equatorial long spacing which started at the yield point for cold-drawn UHMW-PE (which was the only sample for which lamellar scattering was measurable throughout). The decrease in equatorial long spacing can be attributed to lamellar thinning caused by 'fine' chain slip³⁹, as postulated for the MDPE and LLDPE samples which showed similar behaviour¹. Fine slip results in the shearing of lamellar stacks with their normals inclined to the tensile axis, leading to a rotation of the normals away from the tensile axis, coupled with rotation of the chains towards the tensile axis (see Figure 11).

The third piece of evidence for the activation of crystallographic slip at the macroscopic yield point was the activation of the martensitic transformation, in the cold-drawn samples, at the yield point. This argument was previously used to explain the behaviour of the ethylene- α -olefin copolymers¹. Since chain slip is also a plastic deformation mechanism, with a slightly lower CRSS

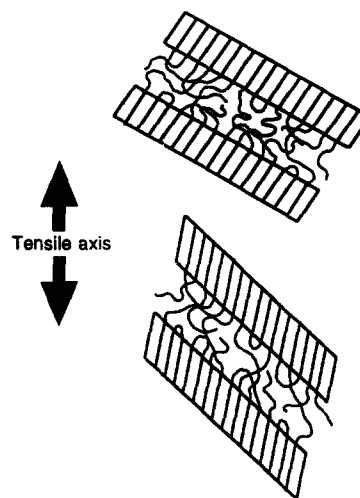


Figure 11 Schematic illustration of the effects of fine slip in lamellae oriented at some angle to the tensile axis. Rotation of the normals away from the tensile axis is coupled with rotation of the chains towards the tensile axis

(albeit determined in single crystal textured PE) than the martensitic transformation, it is expected that, for cold-drawn samples at least, chain slip and the martensitic transformation coexist^{40,41}. So, although there was no direct evidence for chain slip in most of the cold drawn samples, since void scattering overwhelmed the lamellar scattering, chain slip was inferred from the operation of the martensitic transformation coinciding with increasing crystalline orientation.

Finally, the onset of cavitation at the yield point may also be held to indicate the onset of crystallographic deformation mechanisms. Deformation of the amorphous component proceeds until it 'locks up' and is unable to maintain the applied strain⁷. Cavitation releases the constraints and allows crystallographic deformation to proceed during tensile deformation⁷.

The martensitic transformation. The initial study¹¹ on HDPE sample B and LLDPE sample H enabled some conclusions to be drawn regarding the factors governing the occurrence of the martensitic transformation in unoriented PE. In this section the martensitic transformation is reconsidered in more detail using the findings from the more recent studies. Two noticeable features about the monoclinic reflections indicate the mode of martensitic transformation. Firstly, the initial orientation of the monoclinic reflections at the yield point shows that only orthorhombic material in certain orientations is sheared to form the monoclinic phase. It is known from studies of single crystals and thin spherulitic films that different deformation mechanisms are preferred for crystals in different orientations to the tensile axis⁴², and that different mechanisms operate in different regions of spherulites^{43,44}. From the initial orientation of the monoclinic (001) reflection, it is deduced that the martensitic transformation occurred in regions where the lamellar normals were inclined (over a range of angles) to the tensile axis. Chains aligned parallel to the tensile axis probably preferentially slip past each other. Secondly, the direct correlation of the increase in monoclinic ($\bar{2}01$) intensity with the decrease in orthorhombic (110) and (020) intensity, while the orthorhombic (200) reflection remained relatively constant, implied that the martensitic transformation mode was one in which the orthorhombic unit cell was sheared such that the (110) and (020) planes were destroyed but the (200) planes remained the same as a set of Bragg planes in the monoclinic unit cell. Of the four most likely modes given by Bevis and Crellin the T2₂ mode is the most likely candidate, as postulated previously¹¹. Therefore, this paper and the previous investigations^{1,11}, have shown that the martensitic transformation mode is the same regardless of molecular weight, percentage crystallinity, lamellar thickness, branch amount and branch type in unoriented PE.

That the decrease in the equatorial orthorhombic (110) intensity corresponded to the formation of monoclinic material is supported by the behaviour of the (110) reflection in samples deformed at elevated temperatures which did not undergo the martensitic transformation, and which will be described in a subsequent paper⁴⁵. In these samples the (110) intensity increased. Since no orthorhombic material was lost, the normalised intensity scattered throughout the whole of space remained constant, but with increasing orientation more intensity was directed towards the equator, accounting for the increase in (110) intensity. When the martensitic transformation occurred the increasing orientation of the orthorhombic (110) reflection towards the equator was countered by a decrease in the overall

intensity from the orthorhombic material due to phase transformation to the monoclinic phase. Therefore, in the cold-drawn PE, the equatorial orthorhombic (110) intensity decreased and remained at a lower value because there was less orthorhombic material.

The decrease in the monoclinic ($\bar{2}01$) intensity during the load-extension plateau that was observed for certain samples has several possible explanations, which, although detailed previously¹¹, are reconsidered here in the light of more extensive experimental data. The first explanation was that the local stress relaxation due to cavitation causes some monoclinic material, stable only under stress, to revert back to the orthorhombic form. The second explanation was that partial melting occurs. If localised heating during deformation allowed temperatures to exceed 110°C then monoclinic material formed at lower strains would become unstable and revert to the orthorhombic form. The third explanation was that monoclinic material is lost by disruption due to molecular orientation and the overall reduction in percentage crystallinity of the cold-drawn samples.

Cavitation occurs in the amorphous regions whereas the martensitic transformation occurs in the crystalline component. It is possible that sufficient relaxation could occur: a possible inference from the values of percentage crystallinity measured by DSC is that the formation of voids alter the stress field sufficiently to allow the required relaxation in the crystallites. However, cavitation occurs to a greater extent in the annealed samples, witnessed by a larger SAXS intensity during voiding for these samples, yet it was the unannealed HMW-HDPE samples that exhibited the reduction in monoclinic ($\bar{2}01$) intensity. Hence, the amount of voiding does not necessarily relate to the extent of relaxation if cavitation-induced relaxation is responsible for the reduction in monoclinic ($\bar{2}01$) intensity.

Although, according to theory, large temperature rises could occur during adiabatic drawing (leading to instability of the monoclinic phase), it has been proposed that temperatures sufficient to cause melting are unlikely to be reached in cold-drawn samples. However, from the reduction in the amount of monoclinic phase in bulk samples drawn under certain conditions Hendra *et al.*⁴⁶ suggested that local heating is, in fact, sufficient to cause melting and recrystallization. Zhan⁴⁷, who found a similar reduction in intensity of the monoclinic reflections during cold-drawing suggested that local melting caused by the heat of deformation relaxes internal stresses, relieving the crystalline distortion, and allows the monoclinic phase to revert back to the orthorhombic form. If local melting and recrystallization was active then the annealed samples would be expected to show the reduction in monoclinic material. This is because they contain fewer entanglements, allowing more complete relaxation. Comparison of the HMW-HDPE and the UHMW-PE supports this line of reasoning, since no reduction in monoclinic material is observed for the more entangled UHMW-PE. However, the untreated HDPE does not follow the trend. Comparison of the different molecular weight samples discounts the possibility that increasing chain orientation destroys the monoclinic phase. Drawn unannealed HDPE became more oriented than unannealed HMW-HDPE, yet only the latter showed the reduction. It must be concluded then that the reason for the reduction in monoclinic ($\bar{2}01$) intensity remains uncertain.

Strain-softening. Several previous workers have identified deformation at low temperatures with the mechanical

transformation of the lamellar to a fibrillar morphology via shearing and fragmentation of lamellae⁴⁸⁻⁵⁰. The SAXS results from the HMW-HDPE demonstrated that the fibrillar morphology was formed during strain-softening, confirming that the linear PE behaved in the same manner as the ethylene- α -olefin copolymers previously reported¹, in which strain-softening corresponded to the lamellar to fibrillar transition. The increase in cavitation only during strain-softening suggests that voids were formed by the release of constraints during lamellar disruption⁷, supporting a mechanical transition for the fibrillar morphology in cold-drawn samples. At low temperatures the motion of the chains is constrained by entanglements in the amorphous component and their reduced mobility in the crystalline lamellae²⁰. Lamellar fragmentation coupled with cavitation provides a mechanism for the release of these constraints.

During strain-softening the transition from the lamellar to the fibrillar morphology coincided with the orthorhombic (110) four point pattern in the WAXS, this pattern being associated with tilted lamellae^{34,51,52}. Coarse slip on

(hk0)[001] slip systems is generally considered to be the mechanism for lamellar fragmentation^{7,8,53,54}, and is thought to occur after lamellae have maximised the resolved shear stress on them by tilting to a certain orientation⁵¹. The observation of the (110) four point pattern throughout deformation coupled with the absence of a fibre long spacing in UHMW-PE, even though the void scattering was never substantial, supports the proposal that fragmentation of tilted lamellae was responsible for the formation of a fibrillar morphology. The long molecules served to prevent the lamellar structure from fragmenting in the UHMW-PE, and therefore, in the deformation range studied, the lamellae remained intact and tilted, and did not undergo the transition to a fibrillar morphology. In HMW-HDPE and HDPE the lamellae had all fragmented, a fibrillar morphology was formed and the four point pattern was only transient.

The appearance of void scattering on the meridian indicates that initially the voids are extended perpendicular to the tensile axis. During further deformation the elongation of the voids parallel to the tensile axis causes the

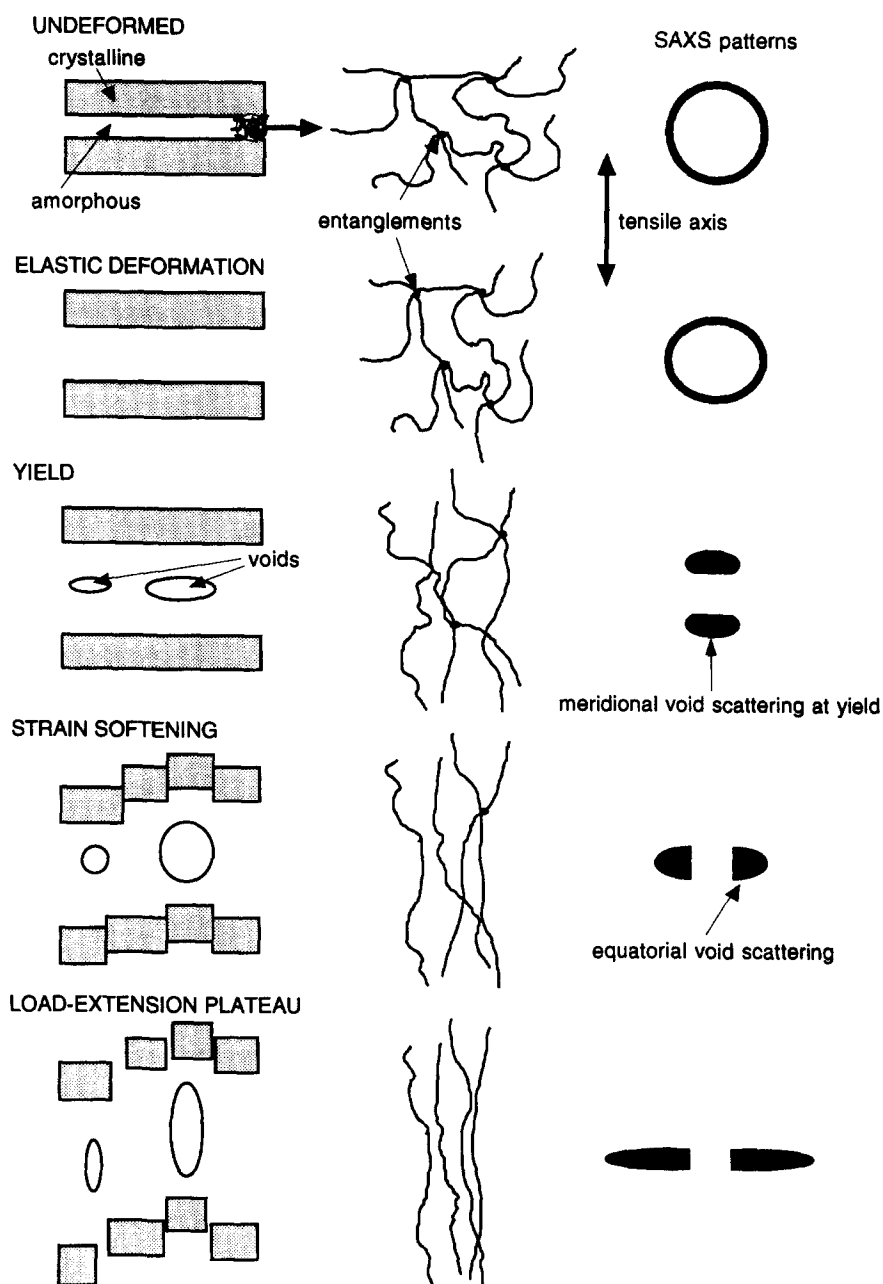


Figure 12 Schematic illustration of the development of cavities in the interlamellar regions during deformation

equatorial streak (the high intensity of which results from the large electron density difference between amorphous PE and voids)⁵⁵. As deformation of the voids proceeds they become longer and thinner, as does the equatorial streak. Figure 12 schematically illustrates a model for how the cavitated structure develops.

The observation that the amount of monoclinic material increased (shown by the increasing intensity of monoclinic reflections) while the number of voids increased showed that the martensitic transformation in bulk HDPE, HMW-HDPE and UHMW-PE samples was associated with the deformation of the lamellae into microfibrils, and therefore high stress conditions.

The load-extension curve plateau. Deformation of the stable fibrillar structure, with no further major structural reorganization in the neck, was responsible for the load-extension curve plateau. Deformation of material in the neck was evidenced by the continued elongation of the voids, but most of the deformation in the plateau probably occurred by drawing of new material into the fibrils. A transition front, extending over a few microns, at the edge of the neck where unoriented material is drawn into the neck, has been observed in similar samples^{56,57}.

The influence of thermal history. The differences between the annealed and unannealed samples may be interpreted in terms of the relative amount of inter- and intralamellar deformation that can occur and the influence of tie molecules^{31,58-60}. Any contribution to the deformation from the amorphous component will be reduced by the increased amount of crystalline material and lower tie molecule density in the annealed samples. The higher yield stresses and lower strains required to activate crystallographic deformation mechanisms in the annealed cold-drawn samples confirm the reduction in importance of the amorphous component in these samples. Therefore, increasing the percentage crystallinity lowers the yield strain since a greater amount of deformation must be borne by the crystalline component responsible for macroscopic yielding.

The lower tie molecule density and reduction in entanglement with increasing crystalline perfection caused the lowest molecular weight HDPE A to become brittle upon annealing³¹.

The influence of molecular weight. The molecular weight dependence can also be explained in terms of the relative proportions of inter- and intra-lamellar deformation and the tie molecule density^{2-6,61}. The increase in percentage crystallinity with decreasing molecular weight increased the amount of deformation borne by the crystalline component, reducing the strain at which crystallographic deformation became operative. The longer molecules in the higher molecular weight samples form an extensive network of tie molecules which inhibits the molecular orientation² and suppresses voiding¹. Therefore, the degree of orientation and amount of cavitation at a given strain decreased with increasing molecular weight. The large degree of entanglement and amount of interlamellar deformation in the UHMW-PE prevented total lamellar disruption in the strain range studied⁶², witnessed by the persistence of the orthorhombic (110) four point pattern, the reduced degree of cavitation and lack of evidence for a fibrillar morphology.

CONCLUSIONS

For all molecular weights the elastic region of the load-extension curve corresponded to deformation mechanisms involving the amorphous component. Interlamellar separation was directly measured and was dependent on the thermal history. The reduced number of tie molecules and increased crystalline perfection of the annealed samples allowed lamellar separation to occur more rapidly. This argument also applies to a comparison of linear polyethylene with ethylene- α -olefin copolymers.

The yield point corresponded to the activation of crystallographic deformation mechanisms. A martensitic transformation, resulting in the conversion of orthorhombic into monoclinic material, occurred at the yield point, coinciding with the formation of microvoids, which formed once the interlamellar regions could no longer sustain the applied strain. The martensitic transformation occurred in lamellae with their normals inclined to the tensile axis and corresponded to the T2₂ mode. Fine chain slip, most probably on the (100)[001] slip system, was observed at the yield point for UHMW-PE which caused lamellar thinning, confirming the basic similarity between the micromechanical behaviour of linear and branched PE, studied previously. Crystallographic deformation mechanisms were activated at lower strains and proceeded to a greater extent in the more crystalline samples (i.e. lower molecular weight and annealed samples) owing to the greater amount of the overall deformation that was borne by the crystalline component.

Fragmentation of the lamellae, once they became tilted to a certain orientation, and loss of constraints caused by cavitation in the amorphous regions caused strain-softening. Local relaxation caused by the loss of constraints was also held to account for a reduction in percentage crystallinity measured in the cavitated samples. The lamellar morphology transformed into a fibrillar one during strain-softening. This was probably the consequence of coarse chain slip. The operation of the martensitic transformation and increase in cavitation only throughout strain-softening, while the fibrillar morphology developed, showed that they occurred at high stress levels and were associated with the formation of the fibrillar morphology at room temperature.

The load-extension curve plateau resulted from steady state drawing of material into the microfibrils, and involved no further major microstructural changes in the neck, although elongation of voids in the necked material was also measured.

ACKNOWLEDGEMENTS

The help of the following people is gratefully acknowledged: Dr Elinor Kerr and Dr Warren Reed, of BP Chemicals, Mary Vickers, of the Department of Materials Science and Metallurgy, University of Cambridge, Pete Bone and Lara Stoimenof, of the Cavendish Laboratory, University of Cambridge, and Mary Heppenstall-Butler, of UMIST. We are indebted to staff at the CCLRC Daresbury Laboratory, including Elizabeth Towns-Andrews, Geoff Mant and Anthony Cleeson, for their technical support which enabled these experiments to be performed and for the provision of programs from the CCP13 software suite which were employed in the data analysis. The financial support of the EPSRC and BP Chemicals is acknowledged.

REFERENCES

- Butler, M.F., Donald, A.M. and Ryan, A.J., *Polymer*, 1997, **38**, 5521–5538.
- Capaccio, G. and Ward, I. M., *Polymer*, 1975, **16**, 239.
- Capaccio, G. and Ward, I. M., *Polymer*, 1974, **15**, 233.
- Capaccio, G., Chapman, T. J. and Ward, I. M., *Polymer*, 1975, **16**, 469.
- Capaccio, G., Crompton, T. A. and Ward, I. M., *Polym. Sci., Polym. Phys. Edn.*, 1976, **14**, 1641.
- Andrews, J. M. and Ward, I. M. J., *Mater. Sci.*, 1970, **5**, 411.
- Lin, L. and Argon, A. S. I., *Mater. Sci.*, 1994, **29**, 294.
- Bowden, P. B. and Young, R. J. J., *Mater. Sci.*, 1974, **9**, 2034.
- Young, R. J., Bowden, P. B., Ritchie, J. M. and Rider, J. G. J., *Mater. Sci.*, 1973, **8**, 23.
- Pope, D. P. and Keller, A. J., *Polym. Sci., Polym. Phys. Edn.*, 1975, **13**, 533.
- Butler, M. F., Donald, A. M., Bras, W., Mant, G. R., Derbyshire, G. E. and Ryan, A. J., *Macromolecules*, 1995, **28**, 6383.
- Hoffman, J. D., Davis, G. T. and Lauritzen Jr., J. I., in *Treatise on Solid State Chemistry*, Vol. 3. Plenum Press, New York, 1976.
- Wunderlich, B. in *Macromolecular Physics*, Vol. 1. Academic Press, New York, 1973.
- Towns-Andrews, E., Berry, A., Bordas, J., Mant, G. R., Murray, P. K., Roberts, K., Sumner, I., Worgan, J. S., Lewis, R. A. and Gabriel, A., *Rev. Sci. Instr.*, 1989, **60**, 2346.
- Bliss, N., Bordas, J., Fell, B. D., Harris, N. W., Helsby, W. I., Mant, G. R., Smith, W. and Towns-Andrews, E., *Rev. Sci. Instr.*, 1995, **66**, 1311.
- Bilsborrow, R. L., Bliss, N., Bordas, J., Cernik, R. J., Clark, G. F., Clark, S. M., Collins, S. P., Dobson, B. R., Fell, B. D., Grant, A. F., Harris, N. W., Helsby, W. I., Smith, W. and Towns-Andrews, E., *Rev. Sci. Instr.*, 1995, **66**, 1633.
- Lee, Y. D., Phillips, P. J. and Lin, J. S., *J. Polym. Sci., Polym. Phys. Edn.*, 1991, **29**, 1235.
- Baltà-Calleja, F. J. and Vonk, C. in *X-ray Scattering of Polymers*. Elsevier, Amsterdam, 1989.
- Varnell, W. D., Harrison, I. R. and Wang, J. I., *Polym. Sci., Polym. Phys. Edn.*, 1981, **19**, 1577.
- Brady, J. M. and Thomas, E. L. J., *Mater. Sci.*, 1989, **24**, 3319.
- Wunderlich, B., in *Macromolecular Physics*, Vol. 3. Academic Press, New York, 1973.
- Peterlin, A. and Meinel, G. J., *Appl. Phys.*, 1965, **36**, 3028.
- Keller, A. and Pope, D. P. I., *Mater. Sci.*, 1971, **6**, 453.
- Kaufman, W. E. and Schultz, J. M. I., *Mater. Sci.*, 1973, **8**, 41.
- Pope, D. P. and Keller, A. I., *Polym. Sci., Polym. Phys. Edn.*, 1975, **13**, 533.
- Peterlin, A. and Meinel, G., *Makromol. Chem.*, 1971, **142**, 227.
- Beresford, D. R. and Bevan, H., *Polymer*, 1964, **5**, 247.
- Slutsker, A. I., Sanphirova, T. P., Yastrebinskii, A. A. and Kuksenko, V. C., *J. Polym. Sci. C*, 1967, **16**, 4093.
- Ishikawa, K., Miyasaka, K., Maeda, K. and Yamada, M. J., *J. Polym. Sci. A2*, 1969, **7**, 1259.
- Crist, B., Fisher, C. J. and Howard, P. R., *Macromolecules*, 1989, **22**, 1709.
- Brown, N. and Ward, I. M. J., *Mater. Sci.*, 1983, **18**, 1405.
- Kennedy, M. A., Peacock, A. J. and Mandelkern, L., *Macromolecules*, 1994, **27**, 5297.
- Lu, X., Qian, R. and Brown, N., *Polymer*, 1995, **36**, 3239.
- Gaucher-Miri, V., François, P. and Séguéla, R. J., *Polym. Sci., Polym. Phys. Edn.*, 1996, **34**, 1113.
- Krause, S. J. and Hosford, W. F. I., *Polym. Sci., Polym. Sci. Edn.*, 1989, **27**, 1853.
- Bartczak, Z., Cohen, R. E. and Argon, A. S., *Macromolecules*, 1992, **25**, 4692.
- Bartczak, Z., Argon, A. S. and Cohen, R. E., *Macromolecules*, 1992, **25**, 5036.
- Bartczak, Z., Argon, A. S. and Cohen, R. E., *Polymer*, 1994, **35**, 3427.
- Peterlin, A. and Meinel, G., *Makromol. Chem.*, 1971, **142**, 227.
- Young, R. J. and Bowden, P. B., *Philos. Mag.*, 1973, **29**, 1061.
- Burnay, S. G., Aere, M. D. D. and Groves, G. W., *J. Mater. Sci.*, 1978, **13**, 639.
- Steidl, J. and Pelzbauer, Z. I., *Polym. Sci.*, 1972, **C30**, 345.
- Allan, P. and Bevis, M., *Philos. Mag.*, 1980, **41**, 555.
- Allan, P. and Bevis, M., *Philos. Mag.*, 1977, **35**, 405.
- Butler, M. F., Donald, A. M. and Ryan, A. J., in preparation.
- Hendra, P. J., Taylor, M. A. and Willis, H. A., *Polymer*, 1985, **26**, 1501.
- Zhan, C. M. J., *Macromol. Sci. Phys. B*, 1991, **30**, 63.
- Sadler, D. M. and Barham, P. J., *Polymer*, 1990, **31**, 36.
- Hoff, M. and Pelzbauer, Z., *Polymer*, 1991, **32**, 999.
- Hoff, M. and Pelzbauer, Z., *Polymer*, 1992, **33**, 4158.
- Brooks, N. W. J., Unwin, A. P., Duckett, R. A. and Ward, I. M., *J. Macromol. Sci. Phys. B*, 1995, **34**, 29.
- Vickers, M. E. and Fischer, H., *Polymer*, 1995, **36**, 2667.
- Galeski, A., Bartczak, Z., Argon, A. S. and Cohen, R. E., *Macromolecules*, 1992, **25**, 5705.
- Adams, W. W., Yang, D. and Thomas, E. L., *J. Mater. Sci.*, 1986, **21**, 2239.
- Grubb, D. T. and Prasad, K., *Macromolecules*, 1992, **25**, 4575.
- Rodríguez-Cabello, J. C., Merino, J. C., Jawhari, T. and Pastor, J. M., *Polymer*, 1995, **36**, 4233.
- Pastor, J. M., Jawhari, T., Martin, B. and Merino, J. C., *Colloid Polym. Sci.*, 1996, **274**, 285.
- Bartczak, Z., Galeski, A., Argon, A. S. and Cohen, R. E., *Polymer*, 1996, **37**, 2113.
- Lu, X. and Brown, N., *Polymer*, 1987, **28**, 1505.
- Lustiger, A. and Markham, R. L., *Polymer*, 1983, **24**, 1647.
- Huang, Y. L. and Brown, N. J., *Polym. Sci., Polym. Phys. Edn.*, 1991, **29**, 129.
- Wilke, W. and Bratrich, M. J., *Appl. Cryst.*, 1991, **24**, 645.